Materials Characterization 207 (2024) 113474

Contents lists available at ScienceDirect

Materials Characterization

journal homepage: www.elsevier.com/locate/matchar

Nano-Y_2O_3 effects on the electrical contact properties of Al_2O_3-Cu/35Cr3TiB_2 composites

Zipeng Ma [a], Meng Zhou [a,*], Baohong Tian [a,b,*], Yi Zhang [a,b,*], Heng Li [a], Xu Li [c], Jin Zou [d], Haoyan Hu [a], Ke Jing [a], Yong Liu [a,b], Alex A. Volinsky [e]

[a] School of Materials Science and Engineering, Henan University of Science and Technology, Provincial and Ministerial Co-construction of Collaborative Innovation Center for Non-ferrous Metals New Materials and Advanced Processing Technology, Luoyang 471023, PR China
[b] Henan Province Key Laboratory of Nonferrous Materials Science and Processing Technology, Luoyang 471023, PR China
[c] Center for Advanced Measurement Science, National Institute of Metrology, Beijing 100029, PR China
[d] Jiangxi Key Laboratory for Advanced Copper and Tungsten Materials, Jiangxi Academy of Sciences, Nanchang 330096, PR China
[e] Department of Mechanical Engineering, University of South Florida, 4202 E. Fowler Ave. ENG 030, Tampa 33620, USA

ARTICLE INFO

Keywords:
Copper-based composites
Electrical contact
Material transfer
Arc energy
Welding force

ABSTRACT

Al_2O_3-Cu/35Cr3TiB_2 and 0.5Y_2O_3/Al_2O_3-Cu/35Cr3TiB_2 electrical contact composites were prepared by vacuum hot pressing sintering *endo*-oxidation method. Both composites were over 98% dense with tensile strengths of 395 MPa and 413 MPa and compressive strengths of 839 MPa and 898 MPa, respectively. The TEM results showed that Cr and TiB_2 particles along with Al_2O_3 nanoparticles generated by internal oxidation were uniformly distributed in the Cu matrix. The addition of Y_2O_3 had almost no negative effects on the electrical conductivity and hardness of the composites. The electrical contact parameters such as arc energy, arc duration, and weld force between pairs of contacts were analyzed. The material transfer direction of both composite contacts was from cathode to anode. The average welding force of the contacts decreased by 24.6% after the addition of Y_2O_3, and the material transfer and loss decreased by 28.6% and 42% at 35 A current, respectively. The addition of Y_2O_3 reduced the arc energy and duration by 43.7% and 55.9% at 25 A and 35 A, respectively, and improved the stability of the contacts during disconnect and closure.

1. Introduction

Electrical contacts are one of the core components of all kinds of instruments and switchgear, mainly responsible for the task of turning on or disconnecting circuits and load currents [1–3]. When the current of the circuit is turned on and off, the arc discharge usually produces a high-temperature arc between the contact pairs, and under the combined action of impact load and thermal energy release, the contacts can fail, exhibiting wear, cracking, arc erosion, and contact welding [4]. With the rapid development of modern industry and the continuous improvement of production levels and power systems automatic controls, traditional contact materials have gradually become unable to meet the more stringent requirements. Therefore, it is of great significance to develop better performance electrical contact materials. In general, the basic requirements of electrical contact materials are: good electrical conductivity and thermal conductivity; low contact resistance; resistance to welding and oxidation; mechanical wear resistance and arc ablation resistance; certain hardness and tensile strength, etc. [5–9]. The mainstream preparation methods of electrical contact materials include powder metallurgy [10,11], internal alloy oxidation [12,13], spark plasma sintering [14], reaction synthesis [15,16], and infiltration [17]. Through comparative studies, it is found that the powder metallurgy method can result in the uniform distribution of reinforcing particles, avoiding the unfavorable factors such as poor bonding due to the non-wetting of the reinforcement and matrix, which makes it the most mature and widely used method for the preparation of particle-reinforced composites.

At present, the copper matrix composites widely used as contacts are Cu-Cr [18–20], Cu-W series [21], and Cu-Mo [22] series alloys. Since the electric coil made of copper is usually seriously oxidized above 300 °C, in order to protect Cu from oxidation at high temperature, Wu et al. [23] prepared thin Cr film by high power and high vacuum arc ion plating,

* Corresponding authors at: School of Materials Science and Engineering, Henan University of Science and Technology, Provincial and Ministerial Co-construction of Collaborative Innovation Center for Non-ferrous Metals New Materials and Advanced Processing Technology, Luoyang 471023, PR China.
E-mail addresses: zhoumeng0902@126.com (M. Zhou), bhtian007@163.com (B. Tian), zhshgu436@163.com (Y. Zhang).

https://doi.org/10.1016/j.matchar.2023.113474
Received 3 September 2023; Received in revised form 11 October 2023; Accepted 13 November 2023
Available online 17 November 2023

which shows good oxidation resistance and excellent thermal stability. Papillon et al. [24] prepared Cu-Cr alloy by powder metallurgy and found that the addition of Cr hinders the sintering kinetics through mechanical effects. It can prevent the expansion phenomena by trapping the released oxygen in the solid chromium oxide, which makes the Cu-Cr more compact and leads to a better combination between Cu and Cr particles. Therefore, Cr has good comprehensive properties to optimize sintering performance and can absorb oxygen at high temperatures to reduce the oxidation of copper-based contacts, which is a key material to improve the breaking capacity of contacts.

In the study of composition and proportioning of copper-based electrical contact materials, most of them will improve the properties and application range of contact composites by adding high melting point metal or ceramic reinforcement [25,26]. Common ceramic reinforcing phases include Al_2O_3, TiB_2, SiC, TiC and WC [27–33]. Fathy et al. [34] prepared Cu-Al_2O_3 composites with different mass fractions by thermochemical technology and powder metallurgy. It is found that Al_2O_3 nanoparticles are uniformly distributed in the copper matrix, and their distribution and quantity determine the thermal conductivity of the composites, and the thermal expansion coefficient of the composites can be effectively reduced by the good combination between the reinforcement phase and the metal matrix. Tian et al. [35] prepared Cu-0.5Al_2O_3 composites by internal oxidation, whose electrical conductivity and softening temperature reached 93% IACS and 800 °C respectively, and the ultimate tensile strength at 600 °C was 172 MPa. It was analyzed that the strengthening mechanism of Al_2O_3 was pinning grain boundaries and subgrain boundaries to inhibit recrystallization of the composites. The above studies have shown that the reinforcement of copper matrix composites by generating uniformly distributed Al_2O_3 nanoparticles within the copper matrix by internal oxidation can obtain high thermal stability while retaining the high electrical and thermal conductivity of the copper matrix to a great extent. TiB_2 has become one of the fastest developing high performance boride ceramics in recent years. It has high electrical wear resistance and lowest resistivity in super-hard ceramics [36–38]. Li et al. [39] prepared Ag-4 wt% TiB_2 contact materials and found that the addition of TiB_2 improved the arc erosion resistance of the contact materials and reduced the amount of material loss and transfer after arc erosion. Pan et al. [40] successfully prepared Cu-Fe-TiB_2 composites by Al-assisted in-situ incorporation of TiB_2 nanophase and purification induced by Fe. The tensile strength and electrical conductivity reached 554 MPa and 62.4% IACS, respectively, realizing a good combination of mechanical and electrical properties. On the one hand, the use of TiB_2 and nano-Al_2O_3 dual-scale ceramic particles to jointly reinforce the copper matrix can optimize the microstructure and thermal stability of the composites. On the other hand, the synergistic effects of different sizes of ceramic particles in the matrix can improve the resistance of the composites to arc erosion during the electrical contact process.

Rare earth elements, also known as “industrial vitamins”, which have unique physical properties and chemical activity, and are often used as trace additives to purify the matrix, refine grains, improve corrosion resistance in materials [41,42]. Zhou et al. [43] prepared nano-Y_2O_3 reinforced Cu-Cr-Y alloys and found that the Y_2O_3 nanoparticles could hinder the grain boundary and dislocation motions, and because of the thermodynamic stability of the Y_2O_3 dispersions and the inhibition of the growth of the Cr particles, the alloys obtained a good combination of strength and thermal conductivity at high temperatures. Mu et al. [44] demonstrated that the addition of Y_2O_3 can inhibit the growth of copper grains and improve the hardness and density of the material, while Y_2O_3 can be more uniformly distributed in the matrix, resulting in improved electrical properties and arc resistance of the samples and the contact resistance of the composite is minimized when 0.5 wt% Y_2O_3 is added. These findings indicate that Y_2O_3 can effectively improve the strength and high-temperature stability of composites, thereby enhancing the electrical contact performance, which is of great significance for the development of contact materials.

Based on the above research, this study decided to adopt the process of ball milling powder mixing and rapid hot-pressing sintering, adding Cr, TiB_2 and nano-Al_2O_3 formed in situ by internal oxidation to strengthen the copper matrix. At the same time, in order to further study the effects of Y_2O_3 on the electrical contact properties of copper matrix composites, Al_2O_3-Cu/35Cr3TiB_2 and 0.5Y_2O_3/Al_2O_3-Cu/35Cr3TiB_2 composites were designed, and their comprehensive properties, microstructure and electrical contact behavior were analyzed and characterized.

2. Experiments

2.1. Composites fabrication

The raw materials for the composites prepared in this paper include Cu-0.4Al (Al 0.4 wt%) alloy powder with an average particle size of 37 μm, Cu_2O 2–5 μm powder, Cr 37 μm powder, 50 nm Y_2O_3 powder of and 3–5 μm TiB_2 powder. The purity of these powders is more than 99.9%, as shown in Fig. 1(a-d). Among them, the addition of Cu-Al and Cu_2O powders is to form dispersed Al_2O_3 particles by internal oxidation in the sintering process, and to strengthen the copper matrix. The addition of Cr, TiB_2 and Y_2O_3 powder is to further improve the strength and electrical contact properties of the composites. The specific process of composites preparation is shown in Fig. 2. First, the powder needed for the preparation of composite materials is weighed according to different proportions (Table 1) and placed into the ball milling jar. Then pure Cu balls of different diameters (the mass ratio of ball to powder is 5:1) are added as grinding medium. Second, the ball mill jar is sealed and placed in a QQM/B light ball mill to grind at the speed of 50 rpm for 6 h to make the powder fully and uniformly mixed as shown in Fig. 1 (e, f). Putting the evenly mixed powder into the graphite mold for a certain degree of prepressing can discharge the air between the powders, increase the heat transfer rate, shorten the heating and curing time and so on. Finally, the graphite mold was placed into FHP-828 fast hot pressing sintering furnace and sintered under 1 Pa vacuum. The specific process parameters are as follows. When the vacuum was lower than 1 Pa, the sintering furnace program was started with heating and applying longitudinal pressure at the same time. The heating rate was 100 °C/min. After 8 min, when the temperature and pressure reach 800 °C and 40 MPa, respectively, the heat was held for 2 min. Then the temperature was raised to 950 °C, and the pressure reached the maximum 45 MPa value, kept for 15 min. Then, there is a cooling process, where the program ends when the temperature and pressure drop to 500 °C and 40 MPa, respectively, after 20 min. The mold is slowly cooled to room temperature with the furnace, and the cylindrical sintered composite of Φ30 mm × 12 mm was obtained.

2.2. Material performance testing

The two ends of the sintered composites were polished smooth with sandpaper of different particle sizes, and polished using the polishing machine to remove the oxide layer, impurities, scratches and other defects that affect the test results on the surface of both ends of the sample. The electrical conductivity of each sample was tested using a digital conductivity meter, and to ensure accurate data, 10 different zones were selected for testing each sample and then the average of these values was taken as the final conductivity of the sample.

The Vickers hardness of each sample was tested by HV-1000 microhardness tester in accordance with the GB/T 4340.4–2022 standard at 300 N load and 10 s loading time. Each sample was tested in 10 different areas and the average values were calculated.

The mass of different samples in air and liquid medium (deionized water at 21 °C) was measured by MS304S densitometer, and the average value was taken after each sample was measured for 5 times. Then the actual density of the composite was calculated by using Archimedes drainage method, and the ratio of the actual density to the theoretical

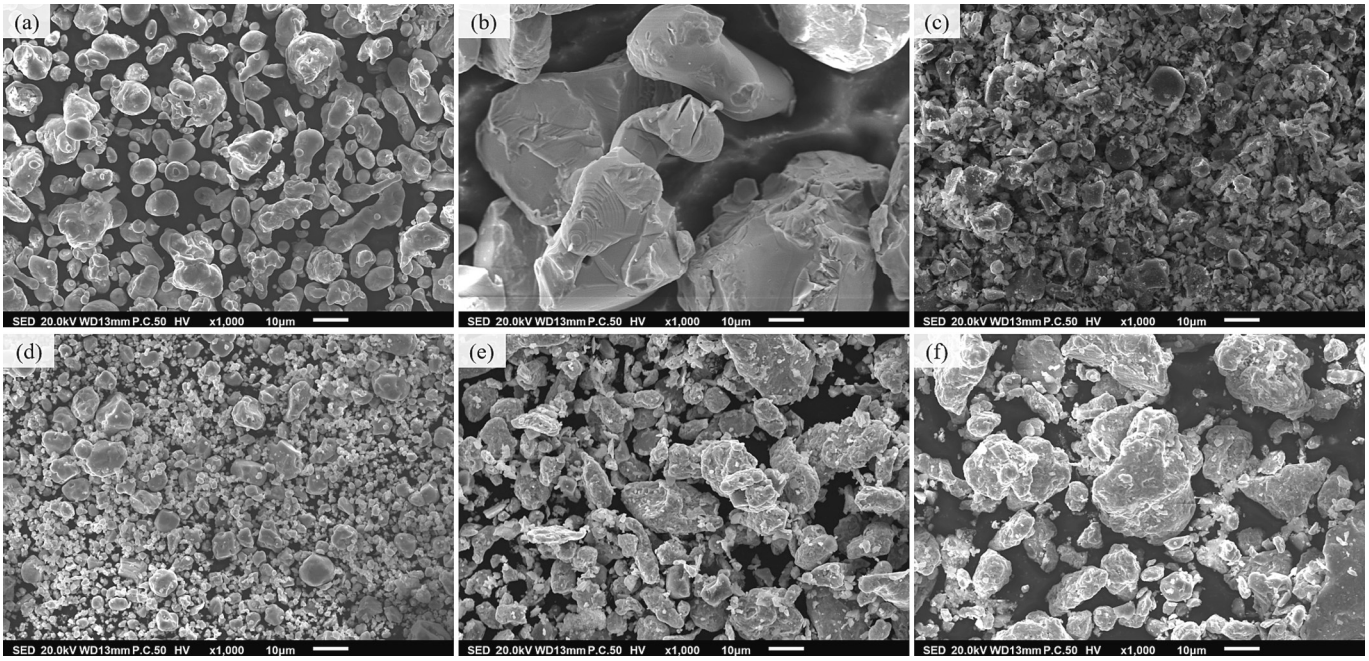

Fig. 1. Scanning electron microscopy images of the feedstock powder: (a) Cu-0.4 wt% Al; (b) Cr; (c) TiB_2; (d) Cu_2O; (e) mixed powder of Al_2O_3-Cu/35Cr3TiB_2; (f) mixed powder of 0.5Y_2O_3/Al_2O_3-Cu/35Cr3TiB_2.

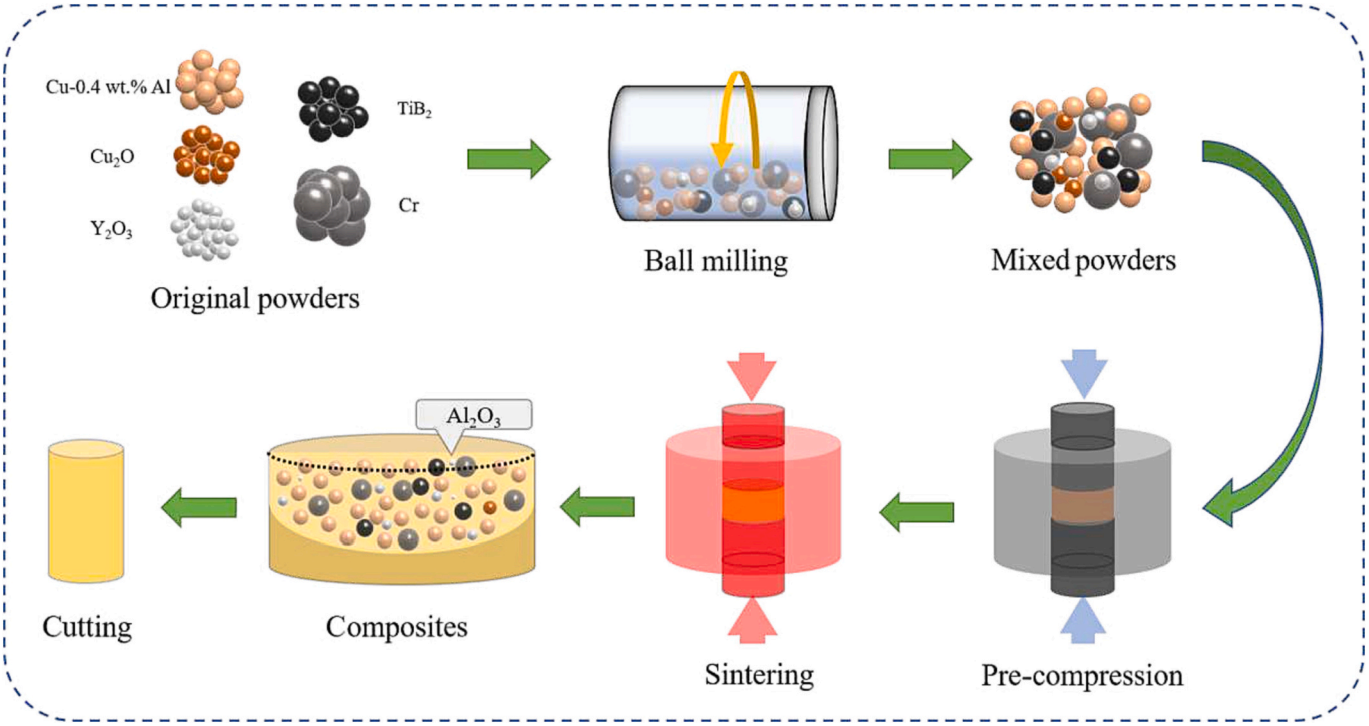

Fig. 2. Preparation process of composite materials.

Table 1
Nominal composition of composites.

Composites	Cu-0.4 wt%Al	Cu_2O	Cr	TiB_2	Y_2O_3
Al_2O_3-Cu/35Cr3TiB_2	59.05	2.95	35	3	0
0.5Y_2O_3/Al_2O_3-Cu/35Cr3TiB_2	58.57	2.93	35	3	0.5

density is the relative density of the composite.

After the sintered composite samples were cut into dog bone shape and Φ8 mm × 10 mm standard samples, the tensile strength and compressive strength of the composites were tested using the AGI-250KN universal testing machine according to the GB/T228.1–2021 and GB/T 7314–2017 standards. The testing rate was 0.2 mm/min, and the average value was taken after each sample was tested three times.

2.3. Electrical contact testing

The sintered composite material is cut into Φ3.8 mm × 10 mm cylindrical electrical contacts, and the surface of the contact samples was polished and placed into ethanol solution to ultrasonically clean it for 15 min, so that the contact surface between the cathode and the anode is smooth and free of oxide layers and impurities, thus ensuring the accuracy and rigor of the electrical contact test. Using the JF04C contact material test system, the electric contact tests were carried out at 25 V constant voltage and 10 A, 20 A, 25 A, 30 A, 35 A current. The whole test was carried out under the protection of argon atmosphere in Fig. 3. The anode was the moving contact and the cathode was the static contacts. The opening and closing of the contacts are regarded as a contact test, and 10,000 electrical contact cycles were conducted for each pair of contacts, and the parameters such as arc energy, arc duration and welding force were monitored in real time. During the test, the closing pressure was maintained between 0.4 N and 0.6 N, and the contact frequency was 1 Hz. The electronic balance with 0.1 mg precision was used to weigh each contact before and after the test. After weighing each contact 5 times, the average value was taken as the final mass of the contact. In order to accurately obtain the mass change of the samples before and after the test, the value of the material loss and transfer during the test is expressed by Δm:

$$\Delta m = m_b - m_a \quad (1)$$

Here, m_a is the mass of the sample before the test, and m_b is the mass of the samples after the test.

2.4. Microstructure characterization

The microstructure of the composites was characterized using a LIBRA-200FE transmission electron microscope, while the surface morphology and elemental distribution of the samples were observed before and after the experiments using a JSM-5610LV and a JSM-7800F scanning electron microscope, and finally, the three-dimensional morphology of the contact surfaces of the samples after arc erosion was established using a PA53MET-3D microscope.

3. Results

3.1. Material properties and microstructure

Table 2 shows the comprehensive properties of the Al_2O_3-Cu/35Cr3TiB_2 and 0.5Y_2O_3/Al_2O_3-Cu/35Cr3TiB_2 composites. Their relative density is above 98%. With the addition of Y_2O_3, the electrical conductivity of the composites slightly decreased, while the microhardness increased to a certain extent. On the one hand, the electrical conductivity of Y_2O_3 is much lower than Cu, so the addition of Y_2O_3 will decrease the electrical conductivity of the composites to a certain extent. On the other hand, the addition of Y_2O_3 will reduce the density of the composites and produce more voids, while voids and hard Y_2O_3 particles will affect the integrity and continuity of the copper matrix and form a stress field in the matrix. All these factors will enhance the electron scatters, thus reducing the electrical conductivity. On the contrary, the hard Y_2O_3 particles in the matrix can pin dislocations to form dislocation cells and hinder the movement of dislocations, thus improving the strength and hardness of the composites.

The sintered samples of two composites were characterized by X-ray diffraction (XRD) with the range of scanning angle and scanning speed of 20° ~ 95° and 1°/min, respectively, and the clear diffraction reflections were obtained in Fig. 4. The diffraction reflections match the expected components, and no impurities reflections such as oxides were found, indicating that the powder was not contaminated by impurities and did not oxidize during sintering. The detected diffraction reflections correspond to (111), (200), (220) and (311) crystal planes of Cu, (110), (200) and (211) crystal planes of Cr, (001) crystal plane of TiB_2, (123) of Al_2O_3 and (112) crystal plane of Y_2O_3, respectively.

Fig. 5 shows the scanning electron microscopy (SEM) backscatter images and energy dispersive X-ray spectroscopy (EDS) analysis results of the two kinds of composites. It can be seen that the structures of the two composites are compact, the copper matrix is continuously distributed, and there are no defects of pores and powder agglomeration. The three initial Cr, TiB_2 and Y_2O_3 phase particles, and the Al_2O_3 nanoparticles formed by internal oxidation are uniformly distributed in the copper matrix. The alumina nanoparticles were successfully scanned at the point scan of Fig. 5(c), and the composition analysis data are shown in Fig. 5(d). From the line scan in Fig. 5(g) and (h), the interface between strengthening phase Cr, TiB_2 particles and Cu matrix is relatively dense, and there is a certain degree of miscibility.

In order to further investigate the microstructure of the composites, the 0.5Y_2O_3/Al_2O_3-Cu/35Cr3TiB_2 contact materials was characterized using transmission electron microscopy (TEM) in Fig. 6. It can be seen from Fig. 6(c) and (d), that the nano-Al_2O_3 and Y_2O_3 are uniformly distributed in the matrix, and these hard particles will pin grain boundaries and sub-grain boundaries and inhibit the dynamic recrystallization of the composites, since the nanoparticles are more concentrated at the grain boundaries in Fig. 6(b). At the same time, these nanoparticles impede the movement of dislocations, which can be seen in Fig. 6(a) where the dislocation density near the hard phase particles increases significantly and causes dislocation stacking, which will lead to an increase in the resistance during the deformation of the matrix, thus improving the strength of the composite. The results after fast

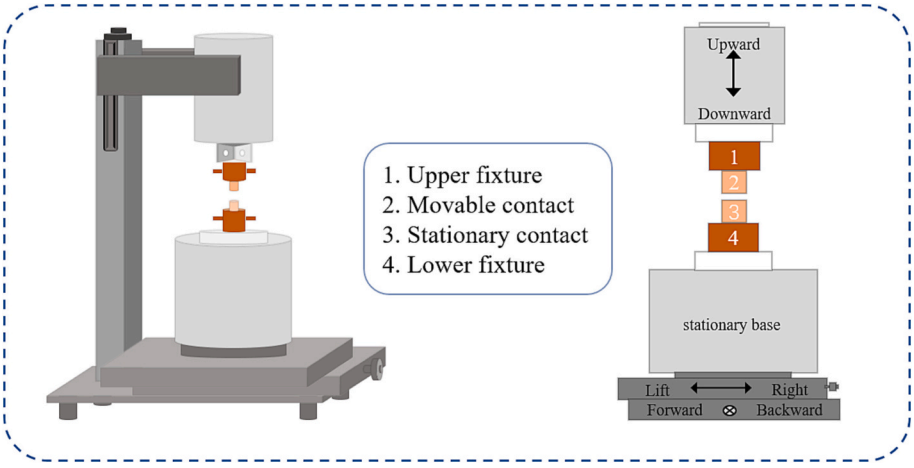

Fig. 3. JF04C contact material testing system schematic diagram.

Table 2
Comprehensive properties of composites.

Composites	Hardness HV	Electrical conductivity % IACS	Relative density %	Tensile strength MPa	Compressive strength MPa
Al_2O_3-Cu/35Cr3TiB_2	174	42.5	98.38	395	839
0.5Y_2O_3/Al_2O_3-Cu/35Cr3TiB_2	178	41.7	98.26	413	898

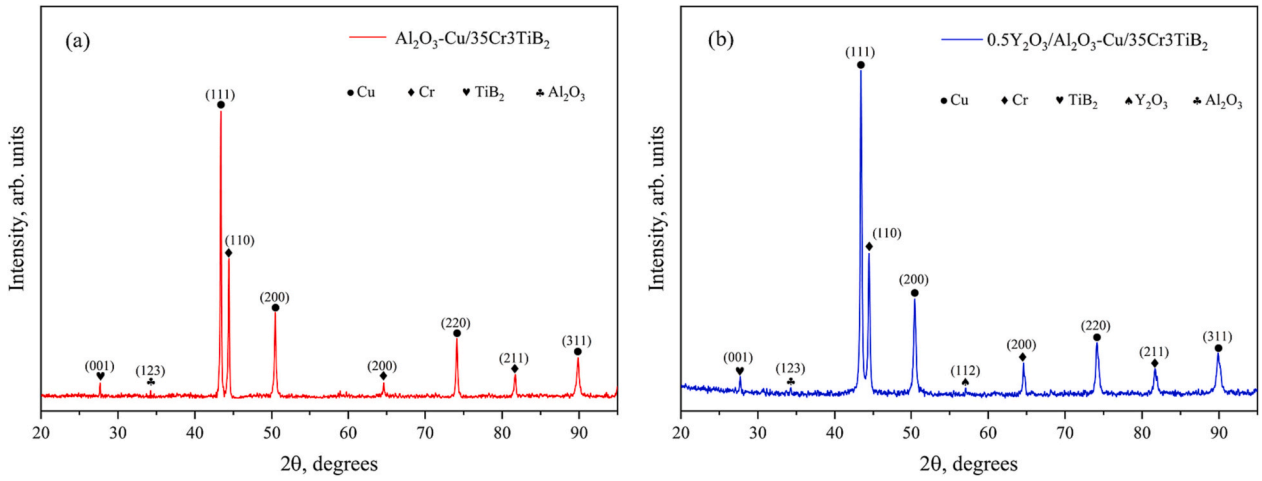

Fig. 4. XRD patterns of the composites: (a) Al_2O_3-Cu/35Cr3TiB_2; (b) 0.5Y_2O_3/Al_2O_3-Cu/35Cr3TiB_2.

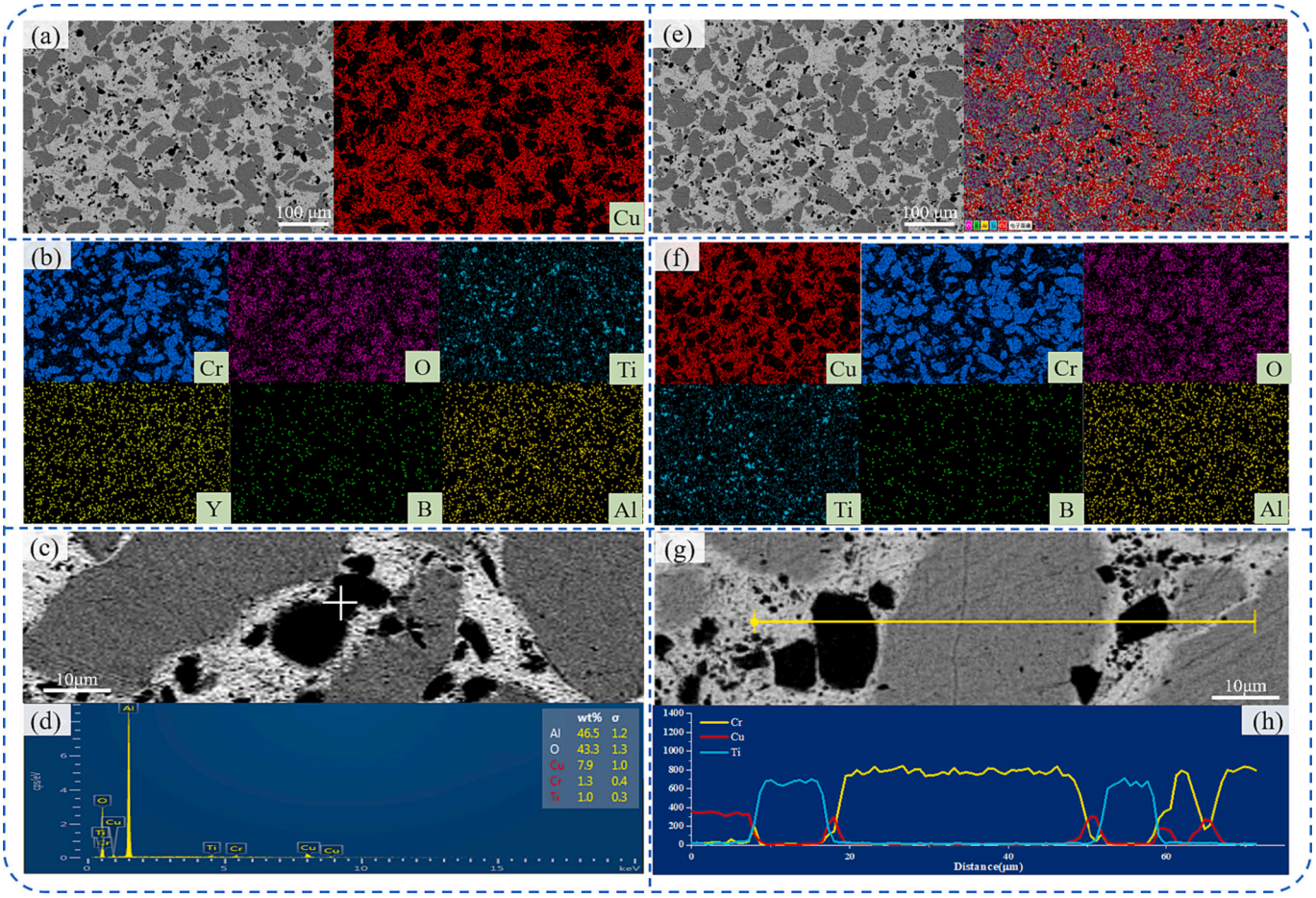

Fig. 5. SEM image and EDS analysis of sintered composites: (a, b) Al_2O_3-Cu/35Cr3TiB_2; (e, f) 0.5Y_2O_3/Al_2O_3-Cu/35Cr3TiB_2.

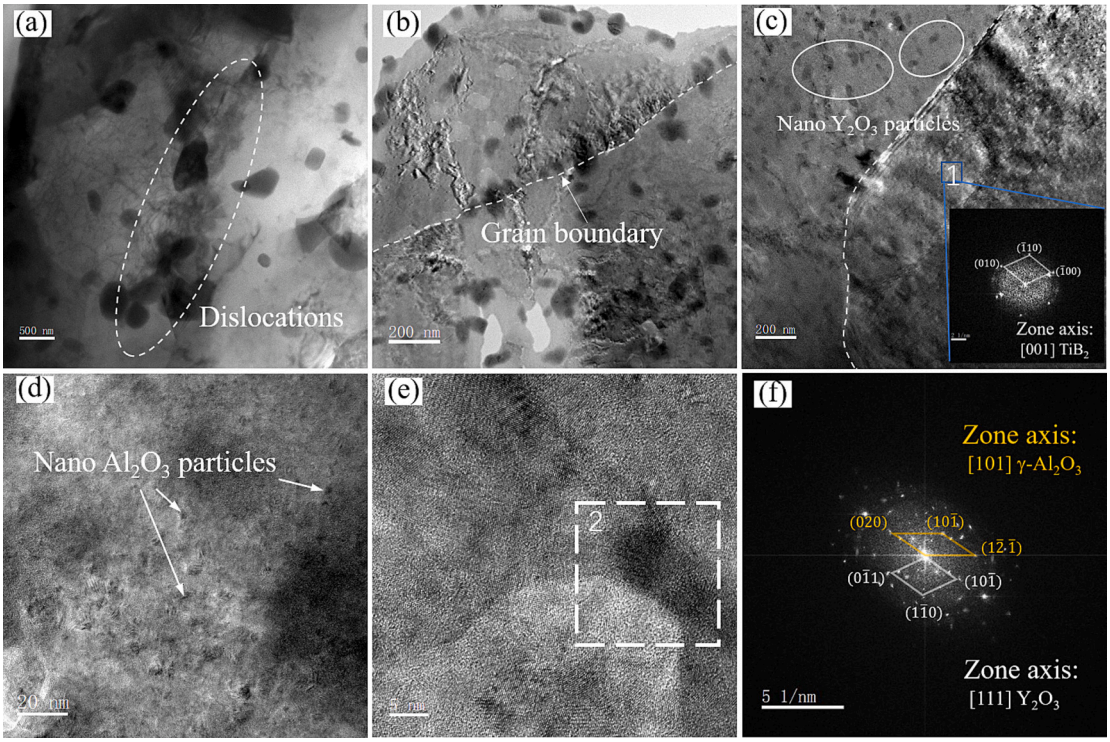

Fig. 6. TEM and HRTEM images of 0.5Y2O3/Al2O3-Cu/35Cr3TiB2 contact materials: (a, b, c, d) TEM images of composite material; (e) HRTEM image of (d); (f) FFT of region 2 of (e).

Fourier transform of the Region 2 in Fig. 6(e) are shown in Fig. 6(f), where the diffraction spots correspond to γ-Al_2O_3 and Y_2O_3, respectively. γ-Al_2O_3 has a high thermal stability and is widely used in many high-temperature and high-pressure environments, so that composites with the Al_2O_3-Cu matrix have become critical materials in the field of electrical contacts. Fig. 6(c) shows the TiB_2 phase distributed in the matrix and the diffraction spots at its Region 1. It can be seen that the bonding state of the copper matrix and TiB_2 particles is good, the interface is clear, and there is no transition layer present.

3.2. Material transfer

Fig. 7 shows the mass change of each contact sample after 10,000 contact tests at different current, as well as the total mass change of each pair of contacts. It can be seen that the mass change of the two kinds of contacts is almost the same, but the change amplitude is different, in which the mass of the anode contacts always increases, while the mass of the cathode contacts always shows a decreasing state, which indicates that the material is transferred from the cathode to the anode during the test, and the amount of increase of the anode can be regarded as the amount of transfer of the material in the test process. At all currents, the total mass of the contact pairs shows a decreasing trend, which means that there is material loss during the test. As the current increases from 10 A to 35 A, the amount of material transfer and loss also tends to increase. In addition, it can be seen from Fig. 7 that the magnitude of the mass change is not steadily increasing as the current rises, rather there is a tendency for a sudden increase at 25 A, after which the increase tends to stabilize.

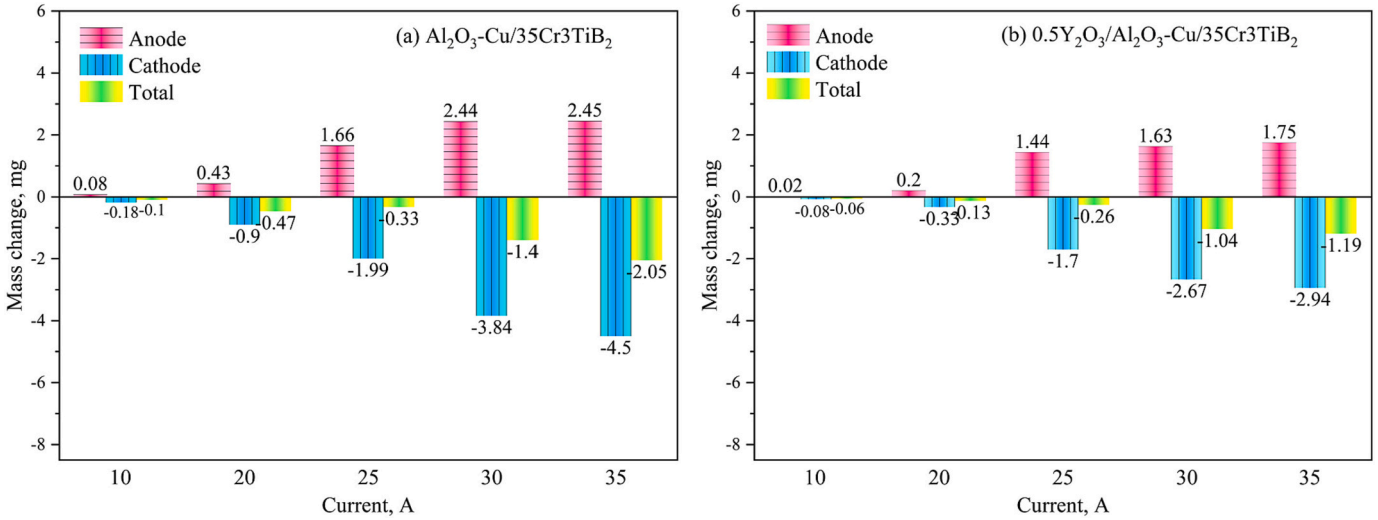

Fig. 7. Mass change of two kinds of contacts under different current conditions: (a) Al_2O_3-Cu/35Cr3TiB_2; (b) 0.5Y_2O_3/Al_2O_3-Cu/35Cr3TiB_2.

The material transfer is realized mainly through the arc transfer and liquid bridge transfer in two ways. The liquid bridge transfer is when the contacts contact discharge, the heat generated will first melt the contacts part, and then because of the surface tension to form a liquid Cu liquid bridge, when the contact pairs is broken, the liquid bridge is elongated until broken, because the fracture is not uniform, resulting in the transfer of materials. Arc transfer refers to the phenomenon that the metal atoms in the contact pairs transfer along the direction of electron movement in the case of arc produced by high current density. That is, it is transferred from the cathode to the anode. As the current rises, the number of liquid bridges and the tendency of arc transfer also rise, resulting in an increase in the material transfer of the contacts. It is worth noting that material transfer is not a single transfer from one contact to another, but a dynamic process of mutual transfer, affected by contact materials and load conditions and other factors. The material loss is because there is a high temperature arc during opening and closing the electrical contact, so that the contact surface temperature rises sharply. When the temperature rises to the melting point or even the boiling point of copper, will lead to the Cu contact surface melting and splashing or evaporation to the surrounding environment. As the current rises, the arc energy generated by the test as well as the instantaneous temperature will also rise simultaneously, so that the loss of contact, evaporation and splashing increases.

In addition, when the current is small, the Joule heat released from the arc is not enough to melt Cu, and at this time, the material transfer mode is mainly arc transfer. However, when the current reaches a level where the heat released from the arc can melt the Cu, the material transfer will be realized through the joint action of the two modes, and thereafter, as the current rises, the liquid bridge transfer gradually dominates. Compared with the arc transfer, the liquid bridge transfer has a greater effect on the contacts mass change. Thus, the reason for the sudden increase in the mass change is that at 20–25 A, the material transfer method of the contacts changes from arc transfer to the synergistic effect of liquid bridge transfer and arc transfer. This phenomenon is also well illustrated by the fact that there is almost no trace of arc erosion on the contact surfaces of contacts with test currents under 20 A. Remarkably, when the current was 20 A, the mass change of the contacts without Y_2O_3 was significantly larger than the contacts with Y_2O_3, which suggested that the Al_2O_3-Cu/35Cr3TiB_2 contacts changed the material transfer mode earlier than the 0.5Y_2O_3/Al_2O_3-Cu/35Cr3TiB_2 contacts as the current was elevated. In other words, Y_2O_3 improves the thermal stability of the composite, which makes the critical current value for the occurrence of the melting phenomenon become larger.

Comparison of Fig. 7(a) and (b) shows that the addition of Y_2O_3 significantly reduces the magnitude of the mass change of the contacts, resulting in lower material transfer and loss. At 30 A and 35 A, the addition of Y_2O_3 decreased the mass transfer of the contacts by 33.2% and 28.6%, respectively, and the material loss during the test decreased by 25.7% and 42%, respectively. This is due to the fact that on the one hand, Y_2O_3 has high thermal stability, which can reduce the melting degree of the composite at high temperature and increase the viscosity of the liquid metal, thus reducing the splashing of liquid droplets and accelerating the fracture of liquid bridges. On the other hand, the low density of Y_2O_3 floats up to the surface of the molten metal liquid,

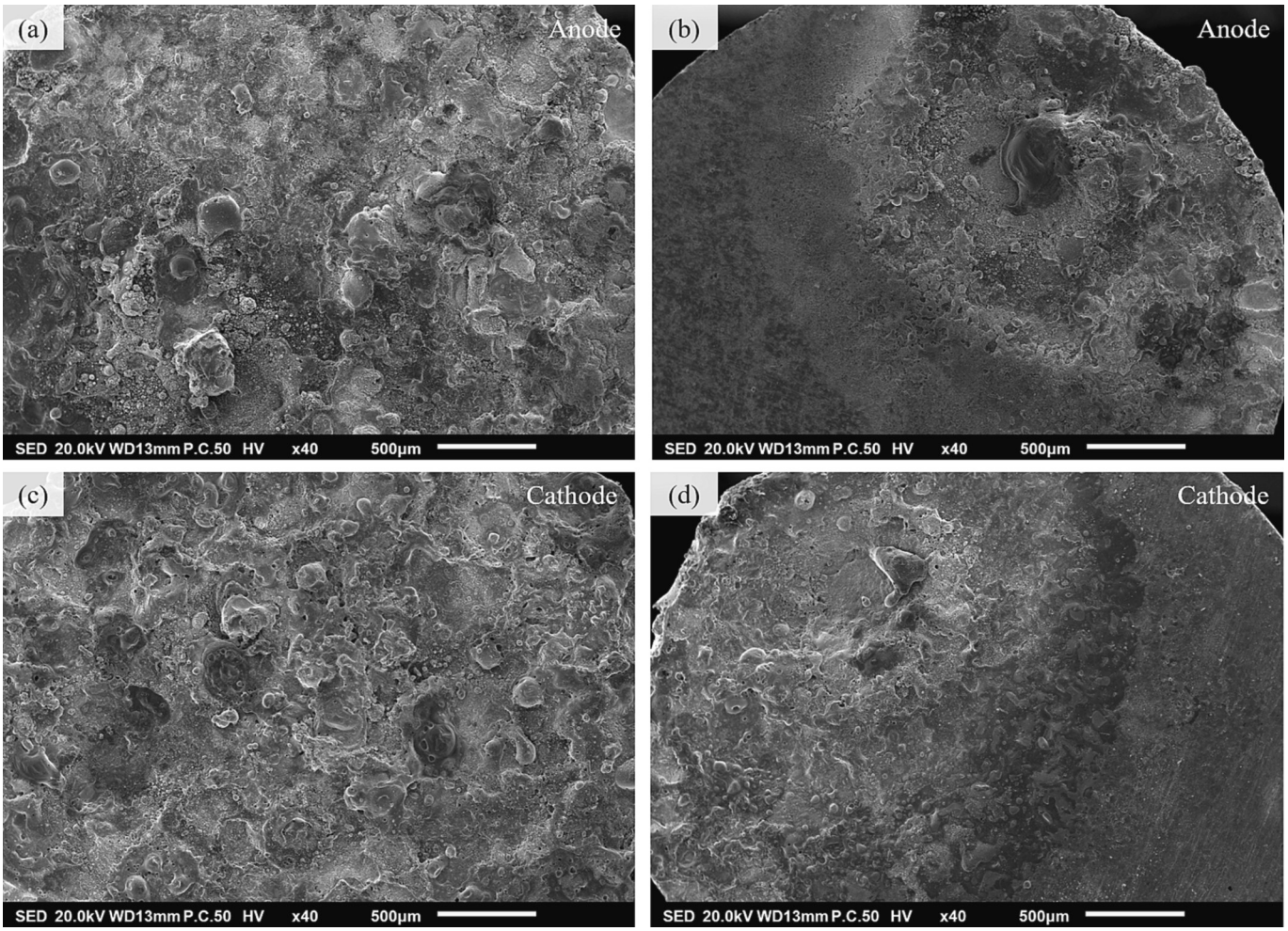

Fig. 8. SEM low magnification images of arc erosion of contacts: (a, c) Al_2O_3-Cu/35Cr3TiB_2; (b, d) 0.5Y_2O_3/Al_2O_3-Cu/35Cr3TiB_2.

hindering the generation of liquid bridges and the splashing of metal droplets, so that the amount of material transfer and loss is reduced.

3.3. Arc erosion

In order to further analyze the mass transfer mechanism of contact materials, the surface of the sample after electrical contact test under DC 25 V and 35 A was characterized by SEM. As shown in Fig. 8, as in the case of several other current test groups, the area and degree of arc erosion of the contacts with $0.5Y_2O_3$ are significantly smaller than without Y_2O_3 at the same voltage and current. Fig. 9 shows the three-dimensional morphology of the contact surfaces of the two kinds of composites after the test under DC 25 V and 35 A. Most of the anode contact surfaces show a raised state, while the cathode has more depressions, and most of them correspond to each other, which further proves that there is material transfer during the contact test process. The height difference between anode and cathode of Al_2O_3-Cu/35Cr3TiB$_2$ contacts after arc erosion is 210 μm and 213 μm, respectively, while for the $0.5Y_2O_3/Al_2O_3$-Cu/35Cr3TiB$_2$ contacts after testing it is 123 μm and 87 μm, respectively. This shows that the addition of Y_2O_3 can effectively improve the arc erosion resistance of the composite.

Fig. 10 shows high-resolution SEM images of the contact surfaces of the samples after the electrical contact tests. It is worth noting that the arc erosion morphology of the two types of contacts is similar, and typical arc erosion morphology such as droplets, bumps, pits, pores, cracks, skeleton and coral-like structures can be seen in Fig. 10, but the addition of Y_2O_3 greatly reduces the degree of arc erosion of the contacts [45,46].The electric arc will be produced in the process of electrical contact, which will increase the local temperature of the contact surfaces. Due to the low melting point of Cu, it first melts, and a small part of it is lost to the surrounding environment. Most of it is left in the low temperature zone of the surfaces and then rapidly solidified to form a droplet-like morphology. The coral structure is caused by the rapid cooling of the molten metal on the contact surfaces after the arc is extinguished, and its main component is Cu, which increases the contact resistance due to the absorption of a large amount of oxygen, which is one of the main reasons for the failure of electrical contacts.

Because the molten Cu absorbs a large amount of gas from the environment, when the contact is disconnected, the temperature of the contact surfaces drops sharply, and the solubility of the gas in the Cu molten pool decreases, which leads to the gas escaping and forming bubbles, which breaks and forms pores after spilling out of the Cu molten pool under the action of pressure difference. If the arc energy is large and the arc lasts for a short time, the bubbles in the molten pool will expand sharply and explosively escape from the molten pool, forming gas eruption pits on the surfaces. At the same time, the existence of pores and gas eruption pits will reduce the mechanical strength and electrical conductivity of the contact surfaces, and it is also the stress concentration area, which can easily cause cracks and promote crack propagation under the action of thermal stress and impact load. The cracks caused by gas eruption pits can be clearly seen in Fig. 10(c). Crack is a very dangerous morphological feature after arc erosion, and it can even lead to large area shedding of contact surfaces. It is the result of the joint action of many factors, and is closely related to the structural properties and external service conditions of the material. According to the comprehensive comparison, it is found that the defects such as pores and cracks on the surface of $0.5Y_2O_3/Al_2O_3$-Cu/35Cr3TiB$_2$ contacts are less than Al_2O_3-Cu/35Cr3TiB$_2$ contacts after arc erosion. In other words, under the same arc erosion, the addition of Y_2O_3 can effectively reduce the droplet splatter on the contact surfaces, and fewer pores and cracks make the contact material have higher stability and longer service life.

Fig. 11 shows the SEM images and EDS analysis results of the anode of the $0.5Y_2O_3/Al_2O_3$-Cu/35Cr3TiB$_2$ contacts after 10,000 electrical contact tests at DC 25 V and 35 A. The oxygen content of the contact surface of the sample after the test increased significantly, because of the high-temperature arc generated during the opening and closing process of the two contacts, and the Joule heat released from the arc increases the temperature of the surfaces, and Cu is easily oxidized to form CuO_2 at higher temperatures. It can be seen from the area scans and line scans that the dominant element in the droplet-like morphology is Cu, and the dominant elements in the skeleton-like structure are Cr and O. Due to the high temperatures generated by the arc, Cu with a low melting point first melts and splashes and forms the droplets. Diffusely distributed Cr particles absorb oxygen at high temperature to form chromium oxide and become viscous semi-molten state, which slowly flows and meets and combines under the action of adhesion and gravity in the process of contact to form a continuously distributed skeleton structure. It can effectively limit the flow and splash of liquid Cu on the contact surfaces

(a, c) Al_2O_3-Cu/35Cr3TiB$_2$; (b, d) $0.5Y_2O_3/Al_2O_3$-Cu/35Cr3TiB$_2$.

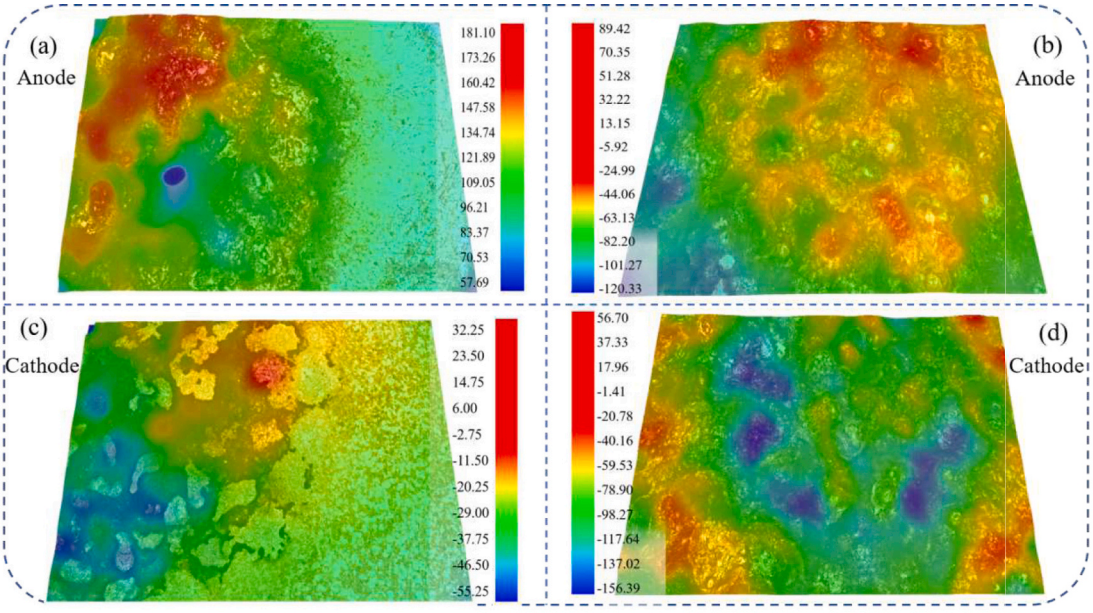

Fig. 9. Three-dimensional morphology of arc erosion of contacts: (a, c) $0.5Y_2O_3/Al_2O_3$-Cu/35Cr3TiB$_2$; (b, d) Al_2O_3-Cu/35Cr3TiB$_2$.

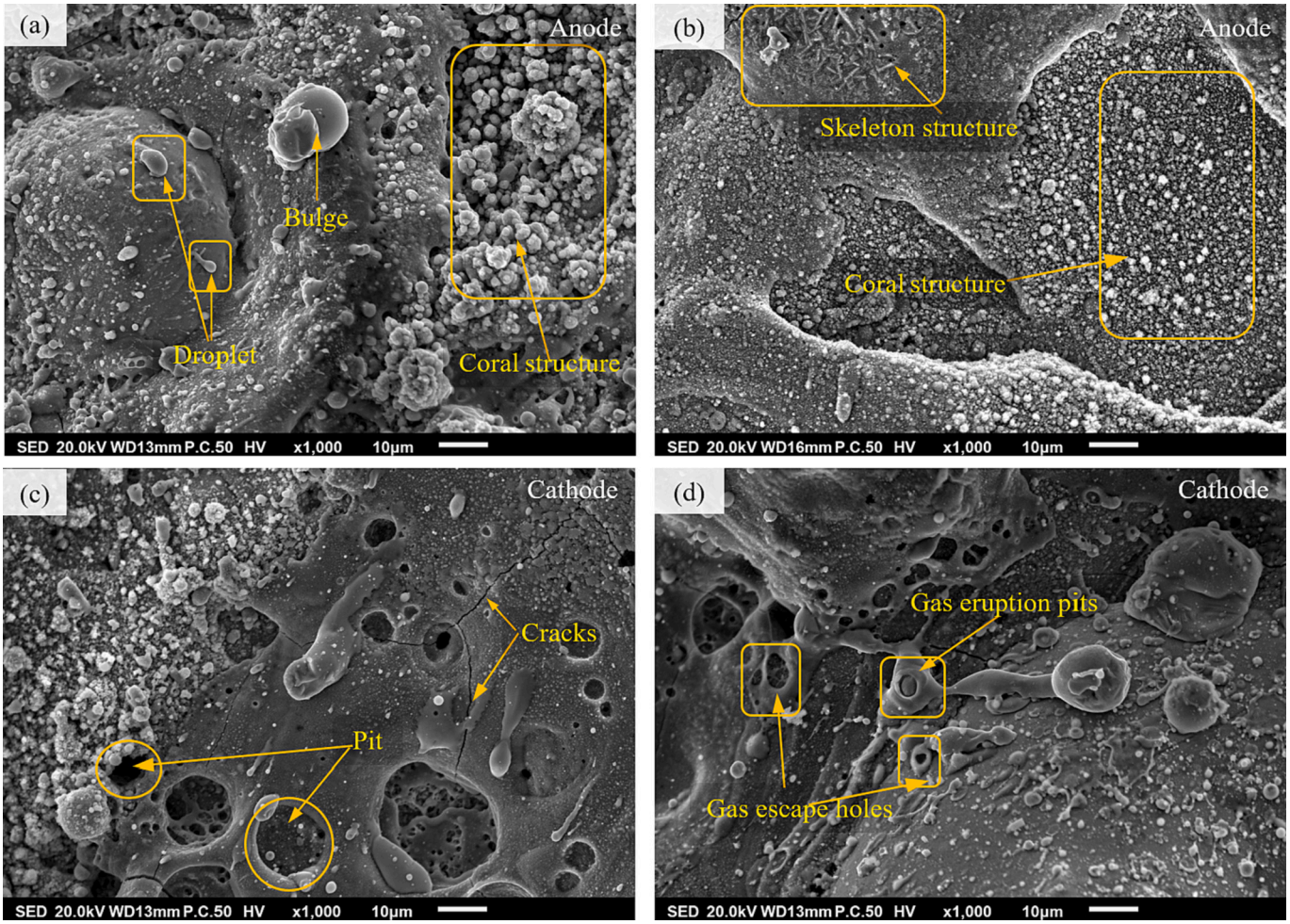

Fig. 10. High magnification SEM images of arc erosion of contacts: (a, c) Al_2O_3-Cu/35Cr3TiB_2; (b, d) 0.5Y_2O_3/Al_2O_3-Cu/35Cr3TiB_2.

and reduce the loss and transfer of material. At the same time, liquid Cu can be stored in the skeleton, which can reduce the quantity and area of Cu liquid when two samples are in contact, reduce the welding between the contacts, and obtain a better breaking capacity. The fine TiB_2 particles and Y_2O_3 nanoparticles in the molten pool can also increase the viscosity of the molten pool and effectively reduce the fluidity of the liquid Cu, so that the contacts can obtain better electrical contact performance.

4. Discussion

4.1. Arc energy and duration

Electrical contact test between the contacts in the arc energy and duration can be a certain degree of description of the material's arc extinguishing ability. The smaller the arc energy, the shorter the arc duration, and the material's arc extinguishing ability is stronger [47,48]. Fig. 12 shows the change of arc energy of two kinds of composite contacts under constant voltage and different current for 10,000 tests, and the arc energy of each 100 tests is averaged as a data point in the figure. Meanwhile, the average value of the total arc energy is added to the graph to facilitate the comparison of the trend of its change. Compared with other composite materials, the arc energy of the two contact materials in this paper is at a lower level. With the increasing current, the average arc energy also increases. As seen in Fig. 12, under the conditions of constant 25 A and 35 A current, the arc energy of the contacts after adding Y_2O_3 is reduced by 43.7% and 55.9%, respectively, with stronger arc extinguishing ability. With the addition of Y_2O_3, the arc energy of the contacts has a smaller tendency to float up and down in its energy value, which means that the composite material is more stable. If the contact is less affected by the arc erosion, then in the state of arc erosion, its conductivity and other properties will be more stable, which can effectively reduce the defects of contact failure due to non-conductivity. In other words, compared with Al_2O_3-Cu/35Cr3TiB_2 contacts, 0.5Y_2O_3/Al_2O_3-Cu/35Cr3TiB_2 contacts can withstand a greater arc energy, that is, they can load a greater current in the stable state.

In order to further analyze the relationship between the arc energy and arc duration, the arc energy of each contact test as the vertical coordinate and arc duration as the horizontal coordinate were mathematically fitted in Fig. 13, and the correlation coefficients of the fitted equations, R^2, were all greater than 0.99. The arc energy and arc duration of different materials at different currents all show a certain linear relationship. Therefore, the addition of Y_2O_3 also reduced the arc duration of the contacts by 43.7% and 55.9% at 25 A and 35 A current, respectively. With the increase of current, the slope of the fitted equation has a tendency to increase. This is due to the fact that under the same arc duration, the arc energy released increases with the current. The slopes of the fitted equations for Y_2O_3 contacts are always lower than f the fitted equations for Al_2O_3-Cu/35Cr3TiB_2 contacts at different current. This indicates that the contacts with added Y_2O_3 have a smaller arc energy for the same arc duration, and the longer the arc duration, the more obvious this trend is. For example, in Fig. 13(a), when the arc duration is T, then the arc energy of the two composite contacts is E_a and E_b, respectively, and E_b is larger than E_a. It is well known that when the arc energy of the material is lower, the speed of extinguishing the arc is

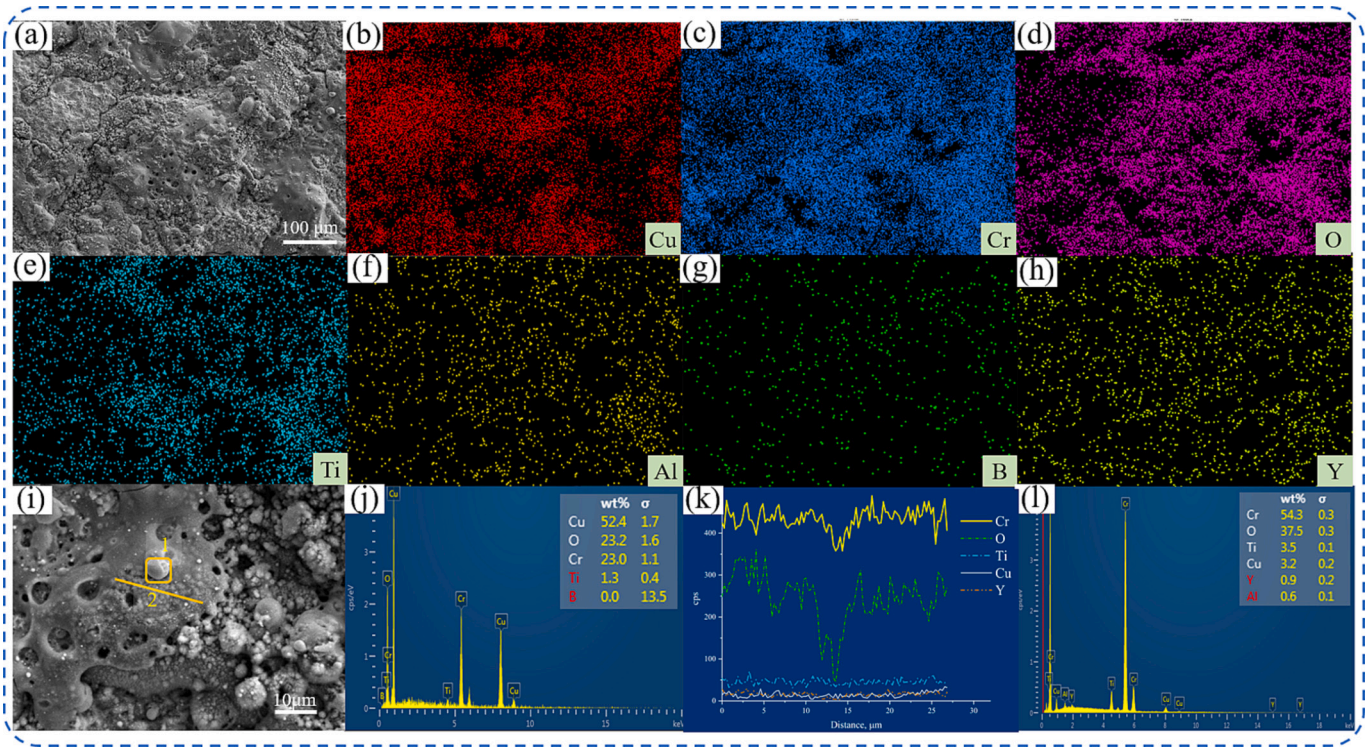

Fig. 11. EDS analysis of the surface of $0.5Y_2O_3/Al_2O_3$-Cu/35Cr3TiB_2 contacts after electrical contact test at 35 A condition: (a, i) BSE images; (b, c, d, e, f, g, h) Element distribution of (a); (j) scan of area 1 of (i); (*k*,*l*) scan of line 2 of (i).

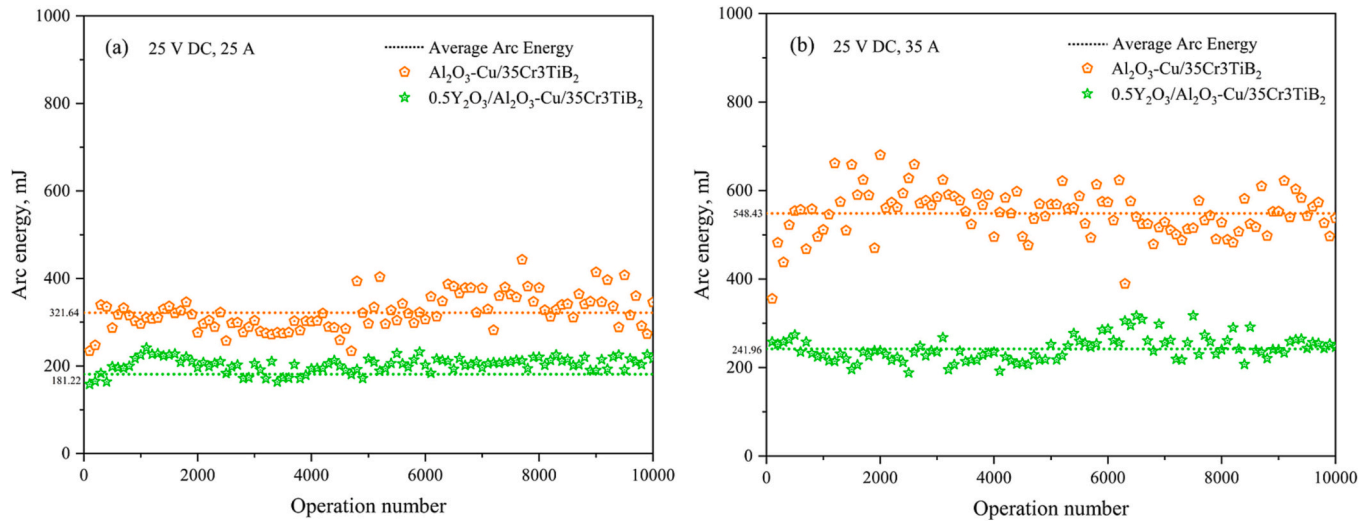

Fig. 12. Changes in arc energy of contacts when tested at different currents: (a) 25 V DC, 25 A; (b) 25 V DC, 35 A.

faster, which means that the arc extinguishing ability of the $0.5Y_2O_3/Al_2O_3$-Cu/35Cr3TiB_2 composite is stronger.

During the experiment, it was found that the arc energy is not the same when the contacts are closed and opened. Therefore, the average opening arc energy and the average closing arc energy of the two composite contacts at different current were calculated in Fig. 14. It was found that the closing arc energy was always greater than the opening arc energy. This is because when the two samples are in contact, it is the process of gradually reducing the contacts spacing. The contact surfaces of the two samples are not completely smooth, and before the load force reaches 0.4–0.6 N, it is always contacted by several raised points first. When the current passes through these contact points and connects the whole circuit, it will increase the current density, produce a larger instantaneous current, and the released arc energy will be larger. On the contrary, when the contacts are disconnected, it is a process of gradually expanding the distance. As part of the contacts Cu has been melted to liquid state by the Joule heat released by the arc, and the resistance of liquid Cu is much greater than the resistance of solid Cu, resulting in an increase in the overall contact resistance of the contacts. With the reduction of the contact area, the arc mainly acts in a smaller area, and the increase in contact resistance, so that the temperature of these areas rapidly rises to the melting point or even the boiling point of the metal. This leads to melting, evaporation and splashing of the material, and most of the energy generated by the arc is dissipated in the form of heat and kinetic energy.

It can be found comparing Fig. 14(a) and (b) that the Y_2O_3 addition

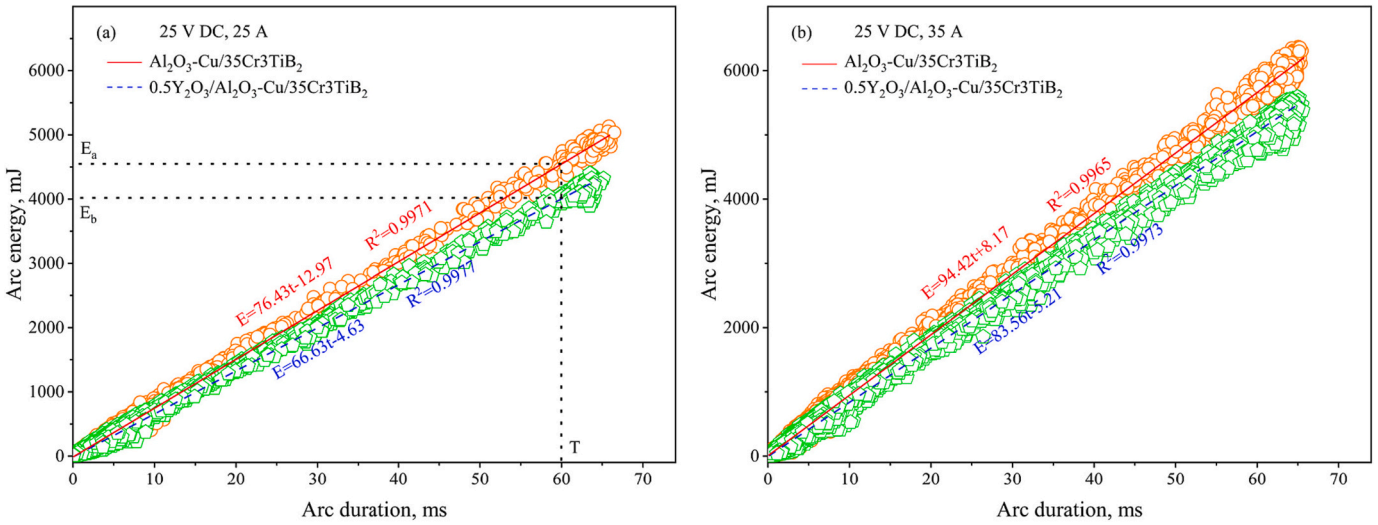

Fig. 13. Relationship between the arc energy and arc duration of contacts: (a) 25 V DC, 25 A; (b) 25 V DC, 35 A.

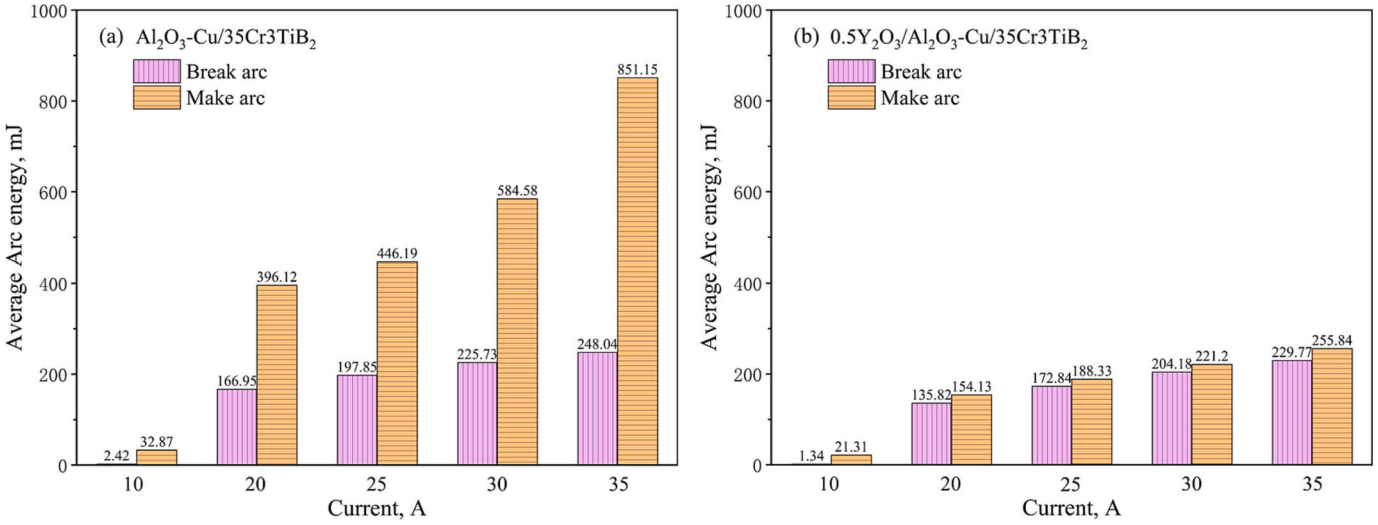

Fig. 14. Average breaking arc energy and closing arc energy of contacts: (a) Al_2O_3-Cu/35Cr3TiB_2; (b) 0.5Y_2O_3/Al_2O_3-Cu/35Cr3TiB_2.

reduces the difference between the closed arc energy and the open arc energy, and the process of opening and closing will be more stable, which can effectively improve the service life of the contacts. When the maximum safe arc energy is certain, the 0.5Y_2O_3/Al_2O_3-Cu/35Cr3TiB_2 contacts can be loaded with a greater current range. For example, when the safe arc energy does not exceed 400 mJ, Al_2O_3-Cu/35Cr3TiB_2 contacts can only load a current of less than 20 A, while contacts with Y_2O_3 can load a current of less than 35 A.

4.2. Welding force

The arc energy is an important factor affecting the welding force of the composites [19,49], Fig. 15 shows the variation of the welding force of the two contacts when tested at different current, after averaging the welding force for every 100 tests as a data point in the figure. The welding force increases accordingly as the current rises, while the welding force of the 0.5Y_2O_3/Al_2O_3-Cu/35Cr3TiB_2 contacts is always lower than the Al_2O_3-Cu/35Cr3TiB_2 contacts for all currents. The reason for this is that more Joule heat is released when the current is elevated, resulting in a consequent increase in the degree and area of melting of the metal on the contact surfaces, and the mixing of the molten metal in the molten state and then cooling it will significantly increase the welding force of the contact pairs. However, the Y_2O_3 addition improves the high-temperature stability of the composites, reduces the area of the metal liquid on the contact surfaces, and decreases the degree of adhesion of the metal liquid, thus reducing the welding force. With the addition of Y_2O_3, the degree of decrease in the average weld force of the contacts at each current ranged from 17.8% to 29%, with an average decrease of 24.6%.

Through the real-time monitoring of the welding force parameters, it was found that the welding force of the Al_2O_3-Cu/35Cr3TiB_2 contacts at higher currents showed a fluctuating increase with the number of tests, and therefore further mathematical fitting of the scatter plots of the variation of the welding force was carried out in Fig. 15(b) and (c). It can be intuitively seen that the slope of the fitted Line for the Al_2O_3-Cu/35Cr3TiB_2 contacts is significantly larger than the 0.5Y_2O_3/Al_2O_3-Cu/35Cr3TiB_2 contacts, which indicates that the average welding force of the Al_2O_3-Cu/35Cr3TiB_2 contacts has a tendency to rise withs the number of tests. However, the slope of the 0.5Y_2O_3/Al_2O_3-Cu/35Cr3TiB_2 contacts is relatively flat, and it can be seen that there is almost no change in the welding force with the number of tests. This is mainly due to the fact that as the number of tests increases, the contact surfaces are more severely eroded by the arc, resulting in an increased degree of surface unevenness. This leads to a reduction in the contact

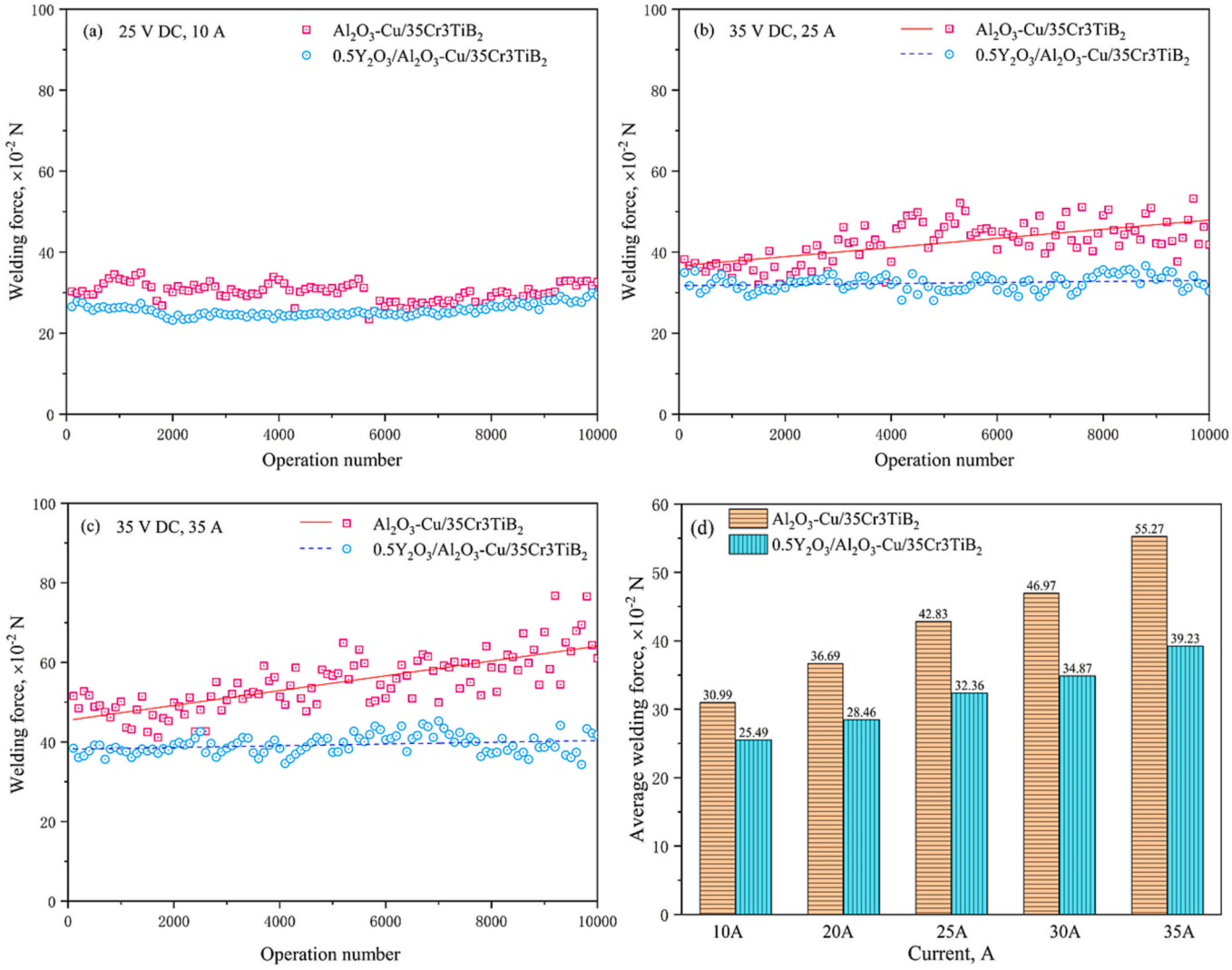

Fig. 15. Variation of welding force of contacts: (a) 25 V DC, 10 A; (b) 25 V DC, 25 A; (c) 25 V DC, 35 A; (d) average welding force of contacts.

area during the test, which increases the current density, releases more Joule heat, and increases the welding force. In contrast, the Y_2O_3 addition resulted in a significant reduction in the degree of arc erosion of the composite material in Fig. (8) and (9), so that the average weld force remained almost unchanged.

It is worth noting that the average welding force of the $0.5Y_2O_3/Al_2O_3$-Cu/35Cr3TiB$_2$ contacts increases significantly less than the Al_2O_3-Cu/35Cr3TiB$_2$ contacts with increasing current, which indicates that the higher the current, the more the welding force of Y_2O_3 contacts decreases, and the more obvious the gap between the two types of contacts' resistance to welding performance. It can be seen from Fig. 15 (a, b, c) that the Y_2O_3 addition makes the welding force fluctuations more stable, which suggests that the contacts with Y_2O_3 have a better breaking capacity, and can effectively reduce the failure phenomenon due to melt welding.

5. Conclusions

(1) Al_2O_3-Cu/35Cr3TiB$_2$ and $0.5Y_2O_3/Al_2O_3$-Cu/35Cr3TiB$_2$ electrical contact composites with relative densities above 98% prepared by rapid hot-press sintering and internal oxidation were characterized by conductivities of 42.5% IACS and 41.7% IACS, microhardnesses of 174 HV and 178 HV, and compressive strengths of 839 MPa and 898 MPa, respectively. The addition of Y_2O_3 had almost no negative effect on the overall performance of the composites.

(2) The microstructure of $0.5Y_2O_3/Al_2O_3$-Cu/35Cr3TiB$_2$ composites was characterized, and the interfacial bonding state of the reinforcing phases Cr and TiB$_2$ particles with the Cu matrix was relatively dense, and the combined effects of the reinforcing phases and the uniformly distributed nanoparticles of γ-Al_2O_3 and Y_2O_3 in the matrix impeded the dislocations' movement and strengthened the comprehensive performance of the composites.

(3) The direction of material transfer was from cathode to anode after electrical contact tests for both Al_2O_3-Cu/35Cr3TiB$_2$ and $0.5Y_2O_3/Al_2O_3$-Cu/35Cr3TiB$_2$ composites, and the addition of Y_2O_3 decreased the degree of material transfer and loss of composites by 28.6% and 42% at 35 A.

(4) The addition of Y_2O_3 decreased the average arc energy and arc duration of the contacts by 49.8%, decreased the average welding force by 24.6%, reduced the degree of arc erosion of the contacts, and improved the stability between the open and closed arc energies, which led to an increase in the range of applications and service life of the contacts.

Declaration of Competing Interest

The authors declare that they have no known competing financial

interests or personal relationships that could have appeared to influence the work reported in this paper.

Data availability

The data that has been used is confidential.

Acknowledgments

This work was supported by the National Natural Science Foundation of China (52071134), the Natural Science Foundation of Henan Province (232300420089), the Technology Innovation Center of Graphene Metrology and Standardization for State Market Regulation (AKYKF2309), the Program for Innovative Research Team at the University of the Henan Province (22IRTSTHN001), the China Postdoctoral Science Foundation (2023TQ0107), Key Research and Development Program of Jiangxi Province (20224BBE52002).

References

[1] D.A. Romanov, V.V. Pochetukha, K.V. Sosnin, S.V. Moskovskii, V.E. Gromov, V. A. Bataev, Y.F. Ivanov, A.P. Semin, Increase in properties of copper electrical contacts in formation of composite coatings based on Ni-C-Ag-N system, J. Mater. Res. Technol. 19 (2022) 947–966, https://doi.org/10.1016/j.jmrt.2022.05.040.

[2] S. Batool, M. Idrees, S.T. Han, V.A.L. Roy, Y. Zhou, Electrical contacts with 2D materials: current developments and future prospects, Small (2023), https://doi.org/10.1002/smll.202206550.

[3] B.J. Wang, Y. Zhang, B.H. Tian, Y.L. Jia, A.A. Volinsky, V. Yakubov, Y. Liu, K. X. Song, M. Fu, Nanoscale precipitates evolution and strengthening mechanism of the aged Cu-Mg-Fe-Sn-P-Y electrical contact wire, J. Mater. Res. Technol. 9 (2020) 6352–6359, https://doi.org/10.1016/j.jmrt.2020.03.051.

[4] C.F. Jia, S.L. Li, X.H. Guo, X. Wang, J.H. Su, K.X. Song, Arc erosion resistance mechanism of Cf-Al_2O_3/Cu composites modified by carbon fibers, J. Mater. Res. Technol. 19 (2022) 4957–4968, https://doi.org/10.1016/j.jmrt.2022.06.173.

[5] S.C. Shu, Q. Zhang, J. Ihde, Q.L. Yuan, W. Dai, M.L. Wu, D. Dai, K. Yang, B. Wang, C. Xue, H.B. Ma, X. Zhang, J.M. Han, X.Y. Chen, C.T. Lin, W.B. Ren, Y.F. Ma, N. Jiang, Surface modification on copper particles toward graphene reinforced copper matrix composites for electrical engineering application, J. Alloys Compd. 891 (2022) 8, https://doi.org/10.1016/j.jallcom.2021.162058.

[6] W.J. Li, Z.Y. Chen, H. Jiang, X.H. Sui, C.F. Zhao, L. Zhen, W.Z. Shao, Effects of interfacial wettability on arc erosion behavior of Zn_2SnO_4/Cu electrical contacts, J. Mater. Sci. Technol. 109 (2022) 64–75, https://doi.org/10.1016/j.jmst.2021.08.045.

[7] R. Cui, Y. Han, Z.X. Zhu, B.A. Chen, Y. Ding, Q. Zhang, Q. Wang, G. Ma, F. Pei, Z. G. Ye, Investigation of the structure and properties of electrodeposited Cu/graphene composite coatings for the electrical contact materials of an ultrahigh voltage circuit breaker, J. Alloys Compd. 777 (2019) 1159–1167, https://doi.org/10.1016/j.jallcom.2018.11.096.

[8] F. Robert, Prediction of contact length, contact pressure and indentation depth of au/carbon nanotube composite micro electrical contact using finite element modeling, Appl. Surf. Sci. 489 (2019) 470–476, https://doi.org/10.1016/j.apsusc.2019.05.169.

[9] Z.J. Lin, W.H. Gao, S.Y. Li, Q. Shen, P.Q. Dai, L.C. Zou, H.X. Chen, X.D. Sun, Effect of in-situ phase transition of (MgCoNiCuZn)O high-entropy oxides on microstructure and performance of Ag-based electrical contact materials, Appl. Surf. Sci. 630 (2023) 11, https://doi.org/10.1016/j.apsusc.2023.157479.

[10] Z.M. Zhang, Z. Li, Z.Q. Tan, H.T. Zhao, G.L. Fan, Y.J. Xu, D.B. Xiong, Z.Q. Li, Bioinspired hierarchical Al_2O_3/Al laminated composite fabricated by flake powder metallurgy, Compos. Pt. A-Appl. Sci. Manuf. 140 (2021) 13, https://doi.org/10.1016/j.compositesa.2020.106187.

[11] Y. Wei, L.M. Luo, H.B. Liu, X. Zan, J.P. Song, Q. Xu, X.Y. Zhu, Y.C. Wu, A powder metallurgy route to fabricate CNT-reinforced molybdenum-hafnium-carbon composites, Mater. Des. 191 (2020) 10, https://doi.org/10.1016/j.matdes.2020.108635.

[12] Z.B. Niu, Z. Li, P. Xiao, Z.C. Li, J.W. Li, Y. Li, Influence of h-BN as an additive on oxidation behaviour and kinetic characteristics of carbon/carbon composites, Corros. Sci. 160 (2019) 13, https://doi.org/10.1016/j.corsci.2019.108162.

[13] S. Mathieu, S. Knittel, P. Berthod, S. Mathieu, M. Vilasi, On the oxidation mechanism of niobium-base in situ composites, Corros. Sci. 60 (2012) 181–192, https://doi.org/10.1016/j.corsci.2012.03.037.

[14] M. Rossetti, G.D. Falk, A.N. Klein, S.Y.G. Gonzalez, C. Binder, D. Hotza, Plasma-assisted rapid sintering of nanotitania powders, J. Eur. Ceram. Soc. 42 (2022) 1670–1684, https://doi.org/10.1016/j.jeurceramsoc.2021.11.006.

[15] Q. Wu, G.F. Xu, C.W. Zhao, R.Z. Huang, M. Yuan, C.P. Wu, Influence of preparation technology on the microstructure and properties of Ag/$SnO_2Bi_2O_3CuO$ composite materials, Mater. Charact. 183 (2022) 14, https://doi.org/10.1016/j.matchar.2021.111537.

[16] Y.H. Jiang, C. Wang, S.H. Liang, J.Q. Ren, X. Du, F. Liu, TiB_2(-TiB)/Cu in-situ composites prepared by hot-press with the sintering temperature just beneath the melting point of copper, Mater. Charact. 121 (2016) 76–81, https://doi.org/10.1016/j.matchar.2016.09.038.

[17] S.A. Hosseinizadeh, A. Pourebrahim, H. Baharvandi, N. Ehsani, Synthesis of nano-layered Ti_3SiC_2 MAX phase through reactive melt infiltration (RMI): Metallurgical and thermodynamical parameters, Ceram. Int. 46 (2020) 22208–22220, https://doi.org/10.1016/j.ceramint.2020.05.298.

[18] Z. Shen, Z.Z. Lin, P.J. Shi, J.L. Zhu, T.X. Zheng, B. Ding, Y.F. Guo, Y.B. Zhong, Enhanced electrical, mechanical and tribological properties of Cu-Cr-Zr alloys by continuous extrusion forming and subsequent aging treatment, J. Mater. Sci. Technol. 110 (2022) 187–197, https://doi.org/10.1016/j.jmst.2021.10.012.

[19] X.H. Zhang, Y. Zhang, B.H. Tian, J.C. An, Z. Zhao, A.A. Volinsky, Y. Liu, K.X. Song, Arc erosion behavior of the Al_2O_3-Cu/(W, Cr) electrical contacts, Compos. Part B Eng. 160 (2019) 110–118, https://doi.org/10.1016/j.compositesb.2018.10.040.

[20] T.M. Gong, P.P. Yao, X. Xiong, H.B. Zhou, Z.Y. Zhang, Y.L. Xiao, L. Zhao, M. W. Deng, Microstructure and tribological behavior of interfaces in Cu-SiO_2 and Cu-Cr metal matrix composites, J. Alloys Compd. 786 (2019) 975–985, https://doi.org/10.1016/j.jallcom.2019.01.255.

[21] X.R. Wang, S.Z. Wei, L.J. Xu, F. Fang, J.W. Li, K.M. Pan, B. Peng, Effect of sintering temperature on fine-grained Cu-W composites with high copper, Mater. Charact. 153 (2019) 121–127, https://doi.org/10.1016/j.matchar.2019.04.017.

[22] J. Zygmuntowicz, J. Los, B. Kurowski, P. Piotrkiewicz, W. Kaszuwara, Investigation of microstructure and selected properties of Al_2O_3-Cu and Al_2O_3-Cu-Mo composites, Adv Compos Hybrid Mater. 4 (2021) 212–222, https://doi.org/10.1007/s42114-020-00188-8.

[23] J.J. Wu, Y.X. Cheng, M.L. Shen, W. Wang, M. Hu, C. Guo, X.D. Lu, S.L. Zhu, High vacuum arc ion plating Cr film for promoting high temperature applicability of Cu, Corros. Sci. 207 (2022) 9, https://doi.org/10.1016/j.corsci.2022.110575.

[24] A. Papillon, S. Roure, H. Schellekens, J.M. Missiaen, J.M. Chaix, E. Rigal, Investigation on the chemical reactions affecting the sinterability and oxide content of Cu-Cr composites during the solid state sintering process, Mater. Des. 113 (2017) 353–360, https://doi.org/10.1016/j.matdes.2016.09.038.

[25] X.H. Zhang, Y. Zhang, B.H. Tian, Y.L. Jia, M. Fu, Y. Liu, K.X. Song, A.A. Volinsky, X. Yang, H. Sun, Graphene oxide effects on the properties of Al_2O_3-Cu/35W5Cr composite, J. Mater. Sci. Technol. 37 (2020) 185–199, https://doi.org/10.1016/j.jmst.2019.08.014.

[26] L.H. Li, S. Liu, M. Zhou, Y. Zhang, S.L. Liang, J.L. Huang, B.H. Tian, Y.F. Geng, Y. J. Ban, Y. Liu, Y.L. Jia, X. Li, A.A. Volinsky, Microstructure evolution of graphene reinforced Cu/CeO_2/Cr electrical contact materials under thermal deformation behavior, J. Mater. Res. Technol. 18 (2022) 1412–1423, https://doi.org/10.1016/j.jmrt.2022.03.038.

[27] S. Pfeiffer, H. Lorenz, Z.W. Fu, T. Fey, P. Greil, N. Travitzky, Al_2O_3/cu-O composites fabricated by pressureless infiltration of paper-derived Al_2O_3 porous preforms, Ceram. Int. 44 (2018) 20835–20840, https://doi.org/10.1016/j.ceramint.2018.08.087.

[28] H.R. Lin, X.H. Guo, K.X. Song, S.L. Li, J. Feng, X.F. Zhang, M.Q. Feng, Synergistic strengthening effect of tungsten carbide (WC) particles and silicon carbide whiskers (SiCw) on mechanical properties of Cu-Al_2O_3 composite, J. Mater. Res. Technol. 15 (2021) 2837–2847, https://doi.org/10.1016/j.jmrt.2021.09.103.

[29] Y. Ma, A. Addad, G. Ji, M.X. Zhang, W. Lefebvre, Z. Chen, V. Ji, Atomic-scale investigation of the interface precipitation in a TiB_2 nanoparticles reinforced Al-Zn-Mg-Cu matrix composite, Acta Mater. 185 (2020) 287–299, https://doi.org/10.1016/j.actamat.2019.11.068.

[30] Q. Wang, X. Lin, N. Kang, X.L. Wen, Y. Cao, J.L. Lu, D.J. Peng, J. Bai, Y.X. Zhou, M. El Mansori, W.D. Huang, Effect of laser additive manufacturing on the microstructure and mechanical properties of TiB_2 reinforced Al-Cu matrix composite, Mater. Sci. Eng. A 840 (2022) 12, https://doi.org/10.1016/j.msea.2022.142950.

[31] M.R. Akbarpour, S. Alipour, A. Safarzadeh, H.S. Kim, Wear and friction behavior of self-lubricating hybrid Cu-(SiC plus x CNT) composites, Compos. Part B Eng. 158 (2019) 92–101, https://doi.org/10.1016/j.compositesb.2018.09.039.

[32] D.X. Yang, Y. Zhou, X.H. Yan, H.L. Wang, X.G. Zhou, Highly conductive wear resistant Cu/Ti_3SiC_2(TiC/SiC) co-continuous composites via vacuum infiltration process, J. Adv. Ceram. 9 (2020) 83–93, https://doi.org/10.1007/s40145-019-0350-4.

[33] V. Rajkovic, D. Bozic, M.T. Jovanovic, Effects of copper and Al_2O_3 particles on characteristics of Cu-Al_2O_3 composites, Mater. Des. 31 (2010) 1962–1970, https://doi.org/10.1016/j.matdes.2009.10.037.

[34] A. Fathy, O. El-Kady, Thermal expansion and thermal conductivity characteristics of Cu-Al_2O_3 nanocomposites, Mater. Des. 46 (2013) 355–359, https://doi.org/10.1016/j.matdes.2012.10.042.

[35] B.H. Tian, P. Liu, K.X. Song, Y. Li, Y. Liu, F.Z. Ren, Microstructure and properties at elevated temperature of a nano-Al_2O_3 particles dispersion-strengthened copper base composite, Mater. Sci. Eng. A 435–436 (2006) 705–710, https://doi.org/10.1016/j.msea.2006.07.129.

[36] F. Long, X.H. Guo, K.X. Song, S.G. Jia, V. Yakubov, S.L. Li, S.H. Liang, Enhanced arc erosion resistance of TiB_2/Cu composites reinforced with the carbon nanotube network structure, Mater. Des. 183 (2019) 15, https://doi.org/10.1016/j.matdes.2019.108136.

[37] S.L. Li, G. Xiuhua, S.L. Zhang, J. Feng, K.X. Song, S.H. Liang, Arc erosion behavior of TiB_2/Cu composites with single-scale and dual-scale TiB_2 particles, Nanotechnol. Rev. 8 (2019) 619–627, https://doi.org/10.1515/ntrev-2019-0054.

[38] M.X. Guo, K. Shen, M.P. Wang, Relationship between microstructure, properties and reaction conditions for Cu-TiB_2 alloys prepared by in situ reaction, Acta Mater. 57 (2009) 4568–4579, https://doi.org/10.1016/j.actamat.2009.06.030.

[39] H.Y. Li, X.H. Wang, X.H. Guo, X.H. Yang, S.H. Liang, Material transfer behavior of $AgTiB_2$ and $AgSnO_2$ electrical contact materials under different currents, Mater. Des. 114 (2017) 139–148, https://doi.org/10.1016/j.matdes.2016.10.056.
[40] S.H. Pan, T.Q. Zheng, G.C. Yao, Y.T. Chi, I. De Rosa, X.C. Li, High-strength and high-conductivity in situ Cu-TiB_2 nanocomposites, Mater. Sci. Eng. A 831 (2022) 9, https://doi.org/10.1016/j.msea.2021.141952.
[41] C. Li, Q.S. Zhou, M.N. Han, S.H. Sha, Y.T. Luo, X.J. Xu, Effect of rare earth element Er on the microstructure and properties of highly alloyed Al-Zn-Mg-Cu-Zr-Ti alloy, J. Alloys Compd. 956 (2023) 15, https://doi.org/10.1016/j.jallcom.2023.170248.
[42] D.S. Zhou, H.W. Geng, W. Zeng, D.Q. Zheng, H.C. Pan, C. Kong, P. Munroe, G. Sha, C. Suryanarayana, D.L. Zhang, High temperature stabilization of a nanostructured Cu-Y_2O_3 composite through microalloying with Ti, Mater. Sci. Eng. A 712 (2018) 80–87, https://doi.org/10.1016/j.msea.2017.11.105.
[43] Y.J. Zhou, S.M. Yin, Q.L. Zhou, Z.L. Chen, L.H. Xue, H.P. Li, Y.W. Yan, Improving high temperature properties of Cu-Cr-Y alloy by residual Cr particles and nano-Y_2O_3 dispersions, J. Mater. Res. Technol. 21 (2022) 2976–2988, https://doi.org/10.1016/j.jmrt.2022.10.130.
[44] Z. Mu, H.R. Geng, M.M. Li, G.L. Nie, J.F. Leng, Effects of Y_2O_3 on the property of copper based contact materials, Compos. Part B Eng. 52 (2013) 51–55, https://doi.org/10.1016/j.compositesb.2013.02.036.
[45] J. Wang, Y.Q. Kang, C. Wang, J.B. Wang, C. Fu, Resistance to arc erosion characteristics of CuO skeleton-reinforced Ag-CuO contact materials, J. Alloys Compd. 756 (2018) 202–207, https://doi.org/10.1016/j.jallcom.2018.05.018.
[46] J. Ding, W.B. Tian, P. Zhang, M. Zhang, Y.M. Zhang, Z.M. Sun, Arc erosion behavior of Ag/Ti_3AlC_2 electrical contact materials, J. Alloys Compd. 740 (2018) 669–676, https://doi.org/10.1016/j.jallcom.2018.01.015.
[47] J.X. Ding, W.B. Tian, P.G. Zhang, M. Zhang, J. Chen, Y.M. Zhang, Z.M. Sun, Preparation and arc erosion properties of Ag/Ti_2SnC composites under electric arc discharging, J. Adv. Ceram. 8 (2019) 90–101, https://doi.org/10.1007/s40145-018-0296-y.
[48] X.H. Guo, Y.B. Yang, K.X. Song, S.L. Li, F. Jiang, X. Wang, Arc erosion resistance of hybrid copper matrix composites reinforced with CNTs and micro-TiB_2 particles, J. Mater. Res. Technol. 11 (2021) 1469–1479, https://doi.org/10.1016/j.jmrt.2021.01.084.
[49] H.Y. Li, X.H. Wang, Y. Xi, Y.F. Liu, X.H. Guo, Influence of WO_3 addition on the material transfer behavior of the $AgTiB_2$ contact material, Mater. Des. 121 (2017) 85–91, https://doi.org/10.1016/j.matdes.2017.02.059.